04,09,13

Photoluminescence of hafnium oxide synthesized by atomic layer deposition

© S.V. Bulyansky[1,2], K.I. Litvinova[1,2,¶], E.P. Kirilenko[1], G.A. Rudakov[1], A.A. Dudin[1]

[1] Institute of Nanotechnology of Microelectronics of the Russian Academy of Sciences, Moscow, Russia
[2] Scientific-Manufacturing Complex „Technological Centre", Zelenograd, Russia

[¶] E-mail: litkristy@gmail.com

Received November 10, 2022
Revised November 17, 2022
Accepted November 18, 2022

In this article, we consider defect formation in hafnium oxide, which belongs to high-K-dielectrics and is a promising material in different areas of nano- and optoelectronics. Hafnium oxide, synthesized by the method of atomic layer deposition, usually forms with a significant oxygen deficiency and contains large number of vacancies. The oxygen vacancies characterized by photoluminescence methods. We showed that the electron-phonon interaction greatly influenced on formation of emission bands. In this case, the emission band can't identify only by the emission maximum. We need to calculate such band parameters as heat release and the energy of a purely electronic transition. This energy that can be compared with the results of theoretical calculations from the first principles.

Keywords: hafnium oxide, photoluminescence, electron-phonon interaction.

DOI: 10.21883/PSS.2023.02.55405.524

1. Introduction

Hafnium oxide belongs to high-K group and is considered as one of the replacements for silicon oxide in scaled-down MOSFET. This material has a wide band gap (5.6−5.8 eV), high density (9.68 g/cm^3) and high permittivity (~ 20) [1]. HfO_2 thin films may be used in multilayer optical coatings both in ultraviolet and infrared region due to high refraction index and low absorption [2]. These films are also used as protective coatings due to their hardness and heat resistance [3], this is an important component of high-performance solar cells [4,5].

Various methods have been used for producing thin hafnium oxide, however, in order to achieve good electrical performance, these approaches require synthesis or annealing at high temperatures. Higher temperatures result in polycrystalline films which may consist of various crystalline phases, including monoclinic, cubic, tetragonal and orthorhombic crystal systems [6–9]. On the other hand, these different HfO_x modifications have different k values. Monoclinic phase, which is the most stable in normal conditions, has $k = 20$, while cubic phase, which is metastable, has high $k = 30$, and for HfO_x, which is in a tetragonal modification, the highest value is $k = 35$. Thus, polycrystalline films containing phases with different k may provide lower physical stability of films [6–23], while grains and grain boundaries cause instability and heterogeneity problems in devices. Therefore, amorphous dielectric material is preferable to ensure improved stability of devices, reduce leakage currents and improve homogeneity.

For amorphous hafnium oxide film production, atomic layer deposition (ALD) technology shall be addressed as a promising film deposition method offering benefits in terms of film thickness reproduction accuracy and film uniformity on the substrate surface [5,24,25]. ALD process is based on consecutive surface-controlled reactions driven by chemisorption [26]. Each chemical reaction taking place on the surface is self-limiting, i.e. a reagent/reactant will not react with the previous chemisorbed layer after surface saturation at this cycle stage, even when a reagent/reactant is fed to the reactor chamber during a long time period. After each stage of previous layer exposure to reagent/reactant, reaction by-products are removed with inert gas. The cycles are repeated until the desired layer thickness is achieved. The ALD method was selected due to its ability to ensure precise film thickness and high area uniformity [27–29].

However, hafnium dioxide has several disadvantages. As in any nonstoichiometric compound, volatile component vacancies play the key role in formation of defects in HfO_2. Oxygen vacancies in HfO_2 films often cause oxide charging (so called fixed charge) and create deep local states in the band gap that facilitate growing probability of charge transfer through the film [30]. Oxygen vacancies for bulk zirconium and hafnium dioxides were investigated in [30–33]. In monoclinic HfO_2, oxygen vacancies may be three- (VIII) or four- (VIV)coordinated in accordance with the local hafnium oxide structure. In addition, charge of these vacancies depends on the number of captured electrons. Five charge states of oxygen vacancy with charge from -2 to $+2$ are observed. Other potential defects

in HfO_2 include hafnium vacancies and interstitial oxygen atoms. Compared with oxygen vacancy formation in a monoclinic structure that required breaking of three to four Hf−O bonds, a hafnium vacancy would require seven such bond to be broken and, thus, is less energetically favorable. The presence of interstitial oxygen is possible when there is excessive oxygen and in this case special film treatment is required [33]. Theoretical calculations of defect states in hafnium dioxide were performed in several publications [33–39]. According to [34], HfO_2 conductivity is of n type. Electron transfer involves traps having energy level lower than the bottom of conduction band by 1−1.5 eV. A spin-singlet state of a double charged oxygen vacancy is energetically more favorable than a spin-triplet state [34]. Calculations of oxygen vacancy formation energy has shown that positively charged V_O are more stable when the vacancy is three-coordinated. Negatively charged vacancy states are stable with four coordination [36]. Dinegatively charged oxygen vacancy is thermodynamically unstable [37].

Oxygen vacancies are extensively involved in the emission band formation. In HfO_2 cathodoluminscescence spectra, a blue band with energy 2.7 eV is observed, which is attributed to oxygen vacancies [40]. Correlation between the trap density and cathodoluminscescence intensity, and between the trap density and refraction index. [41] points out the luminescence dependence on the sizes of nanocrystals, which form hafnium oxide film, due to the increased defect concentration on their surfaces. 2.7 eV emission band was also observed in other publications [42–47], where it was noted that this emission band is formed with participation of strong electron-phonon interaction.

It is impossible to characterize optical transitions involving electron-phonon interaction only by energy. It should be taken into account that due to the Franck-Condon effect emission band peak differs from the absorption band peak by a heat release quantity (Δ).

$$h\mu_a = E_0 + S\hbar\omega, \tag{1}$$

$$h\nu_i = E_0 - S\hbar\omega,$$

$$\Delta = h\nu_a - h\nu_i = 2S\hbar\omega,$$

where $2S\hbar\omega$ — is the heat release; E_0 — is the purely electron transition energy; $h\nu_a$ — is the absorption band peak energy; $h\nu_i$ — is the emission band peak energy.

Relation between these quantities is reflected in the configuration and coordinate diagram (Figure 1).

Thus, it is not possible to compare theoretical calculations for energy condition of local states with optical transition energies. Determine heat release and calculate the purely electron transition energy, which can be compared with theoretical calculations. The purpose of this study is to compare thin hafnium oxide films synthesized by the ALD method.

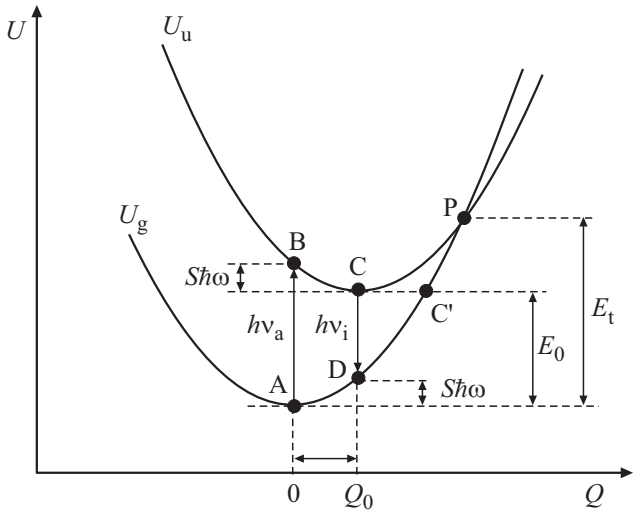

Figure 1. The configuration and coordinate diagram of electron transitions between the defect states according to the electron-phonon interaction. U_g — is the potential energy of ground state, U_u — is the potential energy of excited state, Q — is the generalized coordinate.

2. Test specimens

A 10 nm thin hafnium oxide layer was formed on a single crystal silicon substrate (n-type) by the ALD method. HfO_x film was deposited at a table temperature of 290°C, chamber wall temperature was 130°C. The chemisorption process was carried out by feeding reagent and reactant: $Hf(N(CH_3)_2)_4$ (TDMAH) and H_2O. Metalorganic precursor and water feed pulse duration was 0.4 and 0.1 s, respectively. After the TDMAH pulse feed time, the reactor chamber was purged with argon during 1 s. To ensure saturated vapor pressure requirement, TDMAH temperature was 70°C. TDMAH is a liquid and adhesive metalorganic substance; to avoid sticking to the gas tubes, the precursor supply tubes were heated. Water tank temperature was 20°C, water supply line was preheated up to 120°C.

3. Experimental findings

3.1. HfO_x film structure and composition analysis

Element analysis of HfO_x film thermally deposited on Si was carried out by Auger electron spectroscopy. Primary electron beam voltage was 10 kV, current within — 10 nA at 30° to the specimen surface normal, for spectrum recording, the beam was focused to 100 μm (to reduce the primary current density and specimen degradation during analysis). For the analysis, deposition was performed using argon ions with an energy from 500 to 2000 kV, no preferable deposition of film components was observed.

Two hafnium peaks were recorded on the sample during profile analysis: Hf (MNN) with 1615 eV and Hf(NVV)

peak with 174 eV with the involvement of valence band electrons.

Hf (MNN) was used for the calculations because it better suited the sum of peaks of Hf coupled/non coupled with oxygen. In addition, in different profile points, Hf (NVV) peak changes its form dramatically and differently in different points. This may be indicative of both nonuniform chemical composition and valence band reaction to the positive charge introduction during ion etching.

Figure 2 shows element share in HfO_x film thickness. $HfO_{1.31}$ and metallic Hf are observed in the film. Increased oxygen content in the film is obvious on the surface and at the interface. No silicon and applicable SiO_2 were observed.

It should be noted that the substance distribution analysis at HfO_x film and Si substrate interface has shown that the element atoms were distributed in depth and their interpenetration at the interface was observed. This may be attributed to diffusion processes available during the film growth and to „island“ growth with increased surface roughness.

Thus, the synthesized films contained large number of oxygen vacancies.

X-ray diffraction analysis of thin HfO_x films on Si produced by the ALD method was carried out using Panalitycal Empyrean X-ray diffractometer in CuK_α-radiation with X-ray tube operating conditions 45 kV, 40 mA (Bragg-Brentano focusing arrangement).

Figure 3 shows HfO_x specimen X-ray image obtained using the ALD technique by thermal method. diffraction pattern has no pronounced peaks which means that the structure is X-ray amorphous.

Transmission electron microscopy. The deposited film structure analysis was carried out using Jeol transmission electron microscopy. Bars with deposited hafnium oxide were prepared for the analysis and microphotographs were made for specimen structure characterization in throughout the thickness and on surface. Figure 4 shows a microphotograph of a 10 nm HfO_x specimen made by transmission spectroscopy.

Structural analysis has shown that the HfO_x layer was fully amorphous which is demonstrated by Fourier transform in the selected area.

4. Optical and luminescent properties of HfO_x

Senduro spectral ellipsometer was used to assess the film thickness and uniformity as well as refraction index. The thickness of the produced HfO_x film is 12 nm, 100 mm plate uniformity is about 0.98%. Figure 5 shows the refraction index vs. wavelength. Refraction index at $\lambda = 632.8$ nm is 2.08.

The transmission spectra investigations were carried out using Shimadzu UV-2600 spectrophotometer with integrating sphere, wave range 185–1400 nm. Absorption

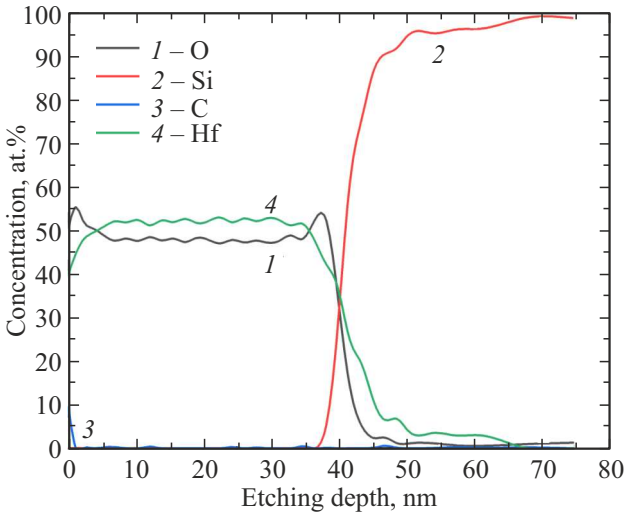

Figure 2. Element concentration profile available in HfO_x specimen prepared by the ALD thermal process on Si substrate.

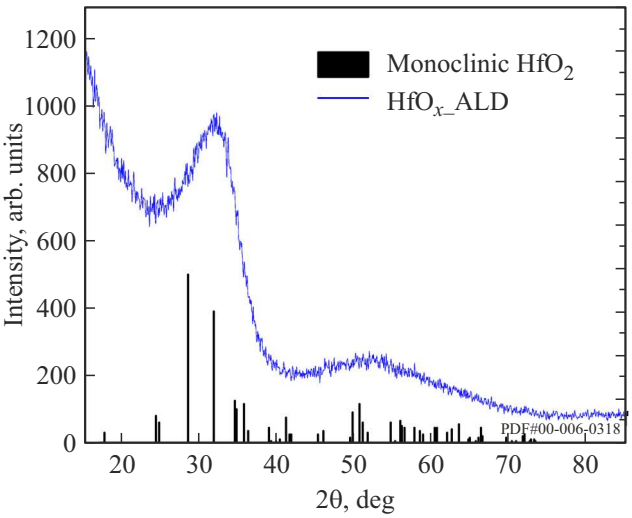

Figure 3. Atomic layer deposited hafnium oxide diffraction pattern.

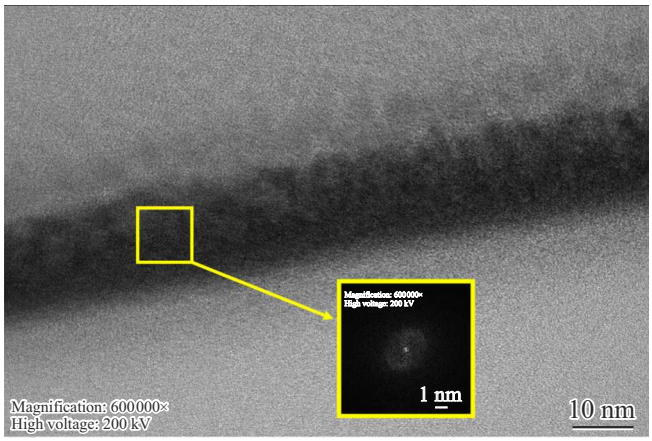

Figure 4. Microphotographs of HfO_x on Si specimen.

spectra were measured on films synthesized in the same conditions as the films on silicon substrate, but the substrate consisted of single crystal silicon. absorption factor is shown in Figure 6. Hafnium oxide is an indirect-bandgap material, therefore the band gap width is calculated using $(\alpha h\nu)^{1/2}$. The band gap width is 5.5 eV. A similar result for the hafnium dioxide band gap was obtained in [47].

Photoluminescence. Photoluminescence spectra were made using inVia Qontor Reneshaw Raman microscope, 325 nm, laser power 200 mW, diffraction grid 1200 mm^{-1}; the measurements were carried out on a liquid-nitrogen-cooled table. The luminescence spectrum is shown in Figure 7. The photon energy excited by 325 nm laser emission was lower than the band gap width and excited no electron-hole pairs. However, this was sufficient to excite the emission.

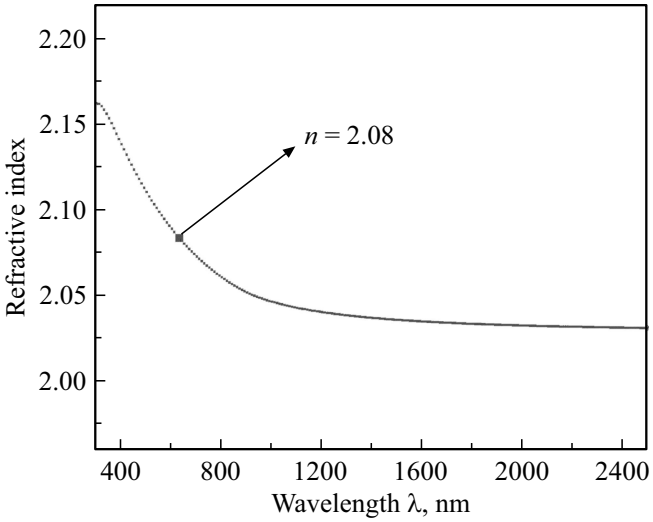

Figure 5. Refraction index vs. wavelength for HfO_x.

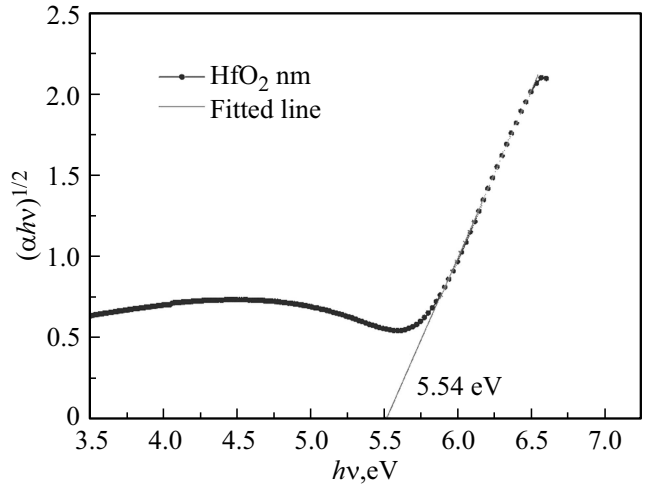

Figure 6. The optical width of the band gap was calculated using the Tauck method [48].

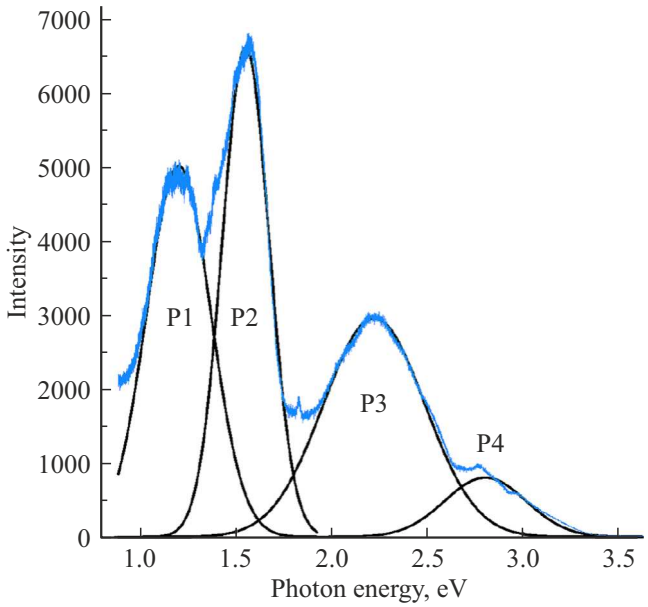

Figure 7. Hafnium oxide photoluminescence spectrum at $T = 173$ K. Thin lines divide the spectrum into separate bands using Gaussian equation.

Emission spectrum is generally a band superposition, with each of them described by the Gaussian distribution:

$$I = \sum_i A_i \exp\left[-\frac{(h\nu - E_i)^2}{2\sigma_i^2}\right], \qquad (2)$$

where A_i — is the emission band amplitude; $h\nu$ — is the current photon energy; E_i — is the emission band center energy; σ_i — is the emission band dispersion.

The emission band approximation by equation (2) makes it possible to determine the emission band peak rather accurately and to find the variance. The emission spectrum was divided into bands by regression method. These parameters for P1–P4 bands are listed in Table 1.

To determine electron-phonon interaction parameters, luminescence spectra were measured at different temperatures. There is low dependence between the variance and

Table 1. Emission band parameters for synthesized hafnium oxide specimens measured at $T = 173$ K

№	$h\nu_i$, eV	σ^2, eV^2	Transitions [40]
P1	1.21	0.028	Intracenter transition between local states V^{-2}
P2	1.56	0.015	Intracenter transition between local states V^{-1}
P3	2.23	0.070	Transition from local state V^{+2} to valence band
P4	2.91	0.040	Transition from local state V^{+1} to valence band

Table 2. Emission band parameters for synthesized hafnium oxide specimens measured at $T = 173$ K

№	$h\nu_i$, eV	$\hbar\omega$, eV	S	E_{P0}, eV	Transition
P1	1.24	0.11	3	0.95	Transition from conduction band to V^{-1} vacancy singlet state
P2	1.56	0.06	3	1.38	Transition from conduction band to singlet V^{-2} vacancy singlet state
P3	2.29	0.12	3	1.95	Intracenter transition of charge state V^{-1} of oxygen vacancy
P5	2.95	0.065	3	2.74	Intracenter transition of charge state V^{-2} of oxygen vacancy

temperature, this means that phonon energy exceeds kT. In this case, electron-phonon interaction parameters are associated with the emission band characteristics as follows [49]:

$$E_i = E_0 + S\hbar\omega, \quad \sigma_i^2 = S(\hbar\omega)^2 \coth\left(\frac{\hbar\omega}{2kT}\right). \qquad (3)$$

The system of equations was solved at several temperatures and the results were averaged. The calculation results are given in Table 2.

The Huang and Rhys factor shows the number of phonons involved in the electron thermalization from point B to C from point D to A (Figure 1). This number is equal to 3. Therefore, the configuration diagram is characterized by a minor polaron shift equal to the square root of this factor. P2 band diagram is shown in Figure 8.

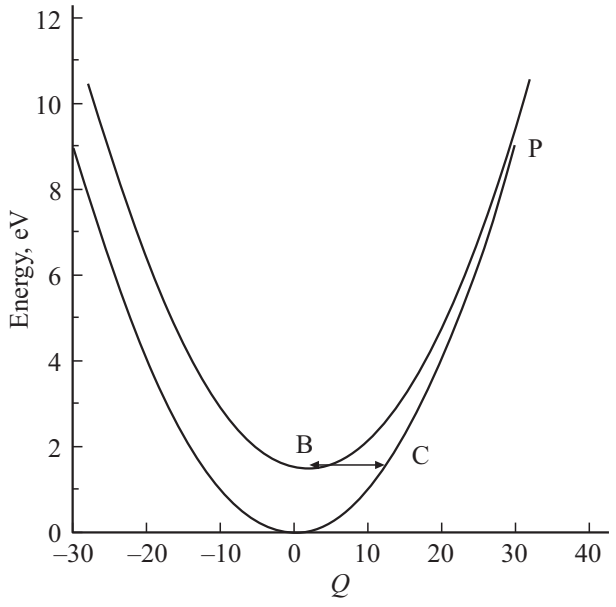

Figure 8. Configuration and coordinate diagram of the center forming emission band P2.

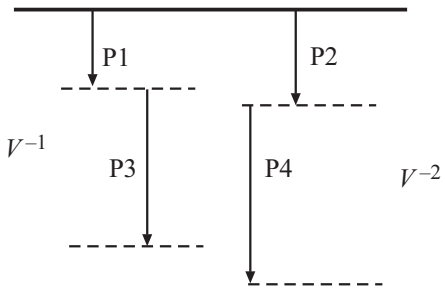

Figure 9. Diagram of emission electron transitions in hafnium oxide.

5. Discussion of findings

According to the diagram in Figure 9, by means of the thermal energy, electron cannot achieve the traditional saddle point P due to the polaron shift. Therefore, the thermal transition between the excited and ground state occurs by tunneling via B−C line. Such transitions are characterized by small capture cross-sections; accordingly, probabilities of recombination through such centers will be low. They play a role of trapping centers. With high concentration of such centers, hopping conduction on their localized states will be observed. Moreover, since the centers have high activation energy, the film can accumulate electrons on these centers and can be charged as it was found in [33].

Oxygen vacancy electron states in various charge states were calculated in [40]. These are the calculations with which the purely electron transition energies should be compared. Negatively charged states form singlet-type split local states in the hafnium oxide band gap. The theoretical calculations show that for oxygen vacancy charge state V^{-1} — energies are 1.29 and 3.46 eV, and for V^{-2} — they have energy 1.46 and 4.17 eV below the bottom of conduction band [40]. It can be assumed that bands P1 (1.24 eV) and P2 (1.56 eV) are attributed to transitions from the conduction band to singlet state of a singly and doubly ionized vacancy. For the singly ionized vacancy state, intracenter transition energy is $3.461.29 = 2.17$ eV, which corresponds to band P3, and for the second — $4.17 - 1.46 = 2.71$ eV. It can be assumed that bands P3 and P4 are attributed to intracenter transitions of singly and doubly ionized vacancies. Transition diagram is shown in Figure 9. Therefore, the main emission bands in hafnium oxide are attributed to electron transitions with the involvement of various oxygen vacancy states. Purely electron transition energies in Table 1 agree with the theoretical calculations [49] and help to interpret the nature of emission bands which are observed experimentally.

6. Conclusion

Hafnium oxide is a promising material for microelectronics, in particular, for submicron gate FET and emit-

ting devices. Hafnium oxide synthesis by atomic layer deposition method gives an X-ray amorphous material with considerable oxygen deficiency. Oxygen vacancy is the main defect that creates local states in the band gap of this material. It can provide five charge states both with deficiency and excess of electrons, and with the excess of electrons, these states are split into two singlet levels. The presence of defects in any charge state in the oxide depends on the oxide formation technique which defines the Fermi level position. luminescence spectra associated with oxygen vacancy were investigated herein, electron-phonon interaction parameters which have critical influence on the emission band shape were calculated, including heat release and purely electron transition energies. These are the energies which shall be reasonably compared with the theoretical ab initio calculations, since the absorption band energies and emissions may be greatly different from the purely electron transition due to high heat release. Such comparison was performed herein and the nature of emission bands was suggested.

Funding

The study was supported by the Ministry of Education and Science of the Russian Federation, project No. 0004-2022-0002, using the unique scientific unit for silicon-carbon technology of heterogeneous integration at the Institute of Nanotechnology of Microelectronics of the Russian Academy of Sciences.

Conflict of interest

The authors declare that they have no conflict of interest.

References

[1] X.-Y. Zhang, C.-H. Hsu, Y.-S. Cho, S. Zhang, S.-Y. Lien, W.-Z. Zhu, F.-B. Xiong. Thin Solid Films **660**, 797 (2018). https://doi.org/10.1016/j.tsf.2018.03.055
[2] L. Gallais, J. Capoulade, J.-Y. Natoli, M. Commandré, M. Cathelinaud, C. Koc, M. Lequime. Appl. Opt. **47**, *13*, C107 (2008). https://doi.org/10.1364/AO.47.00C107
[3] S. Shimada, T. Aketo. J. Am. Ceram. Soc. **88**, *4*, 845 (2005). https://doi.org/10.1111/j.1551-2916.2005.00202.x
[4] H. Geng, T. Lin, A.J. Letha, H.-L. Hwang, F.A. Kyznetsov, T.P. Smirnova, A.A. Saraev, V.V. Kaichev. Appl. Phys. Lett. **105**, *12*, 123905 (2014). https://doi.org/10.1063/1.4896619
[5] J. Wang, S.S. Mottaghian, M.F. Baroughi. IEEE Trans. Electron Devices **59**, *2*, 342 (2012). https://doi.org/10.1109/TED.2011.2176943
[6] J. Robertson. J. Appl. Phys. **104**, *12*, 124111 (2008). https://doi.org/10.1063/1.3041628
[7] P.W. Peacock, J. Robertson. J. Appl. Phys. **92**, *8*, 4712 (2002). https://doi.org/10.1063/1.1506388
[8] J. Robertson. Eur. Phys. J. Appl. Phys. **28**, *3*, 265 (2004). https://doi.org/10.1051/epjap:2004206
[9] J.H. Choi, Y. Mao, J.P. Chang. Mater. Sci. Eng.: R Rep. **72**, *6*, 97 (2011). https://doi.org/10.1016/j.mser.2010.12.001
[10] K. Kukli, M. Ritala, T. Sajavaara, J. Keinonen, M. Leskelä. Thin Solid Films **416**, *1–2*, 72 (2002). https://doi.org/10.1016/S0040-6090(02)00612-0
[11] X. Zhao, D. Vanderbilt. Phys. Rev. B **65**, *23*, 233106 (2002). https://doi.org/10.1103/PhysRevB.65.233106
[12] G.-M. Rignanese, X. Gonze, G. Jun, K. Cho, A. Pasquarello. Phys. Rev. B **69**, *18*, 184301 (2004). https://doi.org/10.1103/PhysRevB.69.184301
[13] W.A. MacDonald. J. Mater. Chem. **14**, *1*, 4 (2004). https://doi.org/10.1039/b310846p
[14] D.E. Mentley. Proc. IEEE **90**, *4*, 453 (2002). https://doi.org/10.1109/JPROC.2002.1002520
[15] H. Yabuta, M. Sano, K. Abe, T. Aiba, T. Den, H. Kumomi, K. Nomura, T. Kamiya, H. Hosono. Appl. Phys. Lett. **89**, *11*, 112123 (2006). https://doi.org/10.1063/1.2353811
[16] K. Nomura, H. Ohta, A. Takagi, T. Kamiya, M. Hirano, H. Hosono. Nature **432**, *7016*, 488 (2004). https://doi.org/10.1038/nature03090
[17] E. Fortunato, N. Correia, P. Barquinha, L. Pereira, G. Goncalves, R. Martins. IEEE Electron Device Lett. **29**, *9*, 988 (2008). https://doi.org/10.1109/LED.2008.2001549
[18] D.C. Paine, B. Yaglioglu, Z. Beiley, S. Lee. Thin Solid Films **516**, *17*, 5894 (2008). https://doi.org/10.1016/j.tsf.2007.10.081
[19] P. Barquinha, G. Gonçalves, L. Pereira, R. Martins, E. Fortunato. Thin Solid Films **515**, *24*, 8450 (2007). https://doi.org/10.1016/j.tsf.2007.03.176
[20] S.-H.K. Park, C.-S. Hwang, M. Ryu, S. Yang, C. Byun, J. Shin, J.-I. Lee, K. Lee, M.S. Oh, S. Im. Adv. Mater. **21**, *6*, 678 (2009). https://doi.org/10.1002/adma.200801470
[21] D.H. Levy, D. Freeman, S.F. Nelson, P.J. Cowdery-Corvan, L.M. Irving. Appl. Phys. Lett. **92**, *19*, 192101 (2008). https://doi.org/10.1063/1.2924768
[22] R.L. Hoffman, B.J. Norris, J.F. Wager. Appl. Phys. Lett. **82**, *5*, 733 (2003). https://doi.org/10.1063/1.1542677
[23] P.F. Carcia, R.S. McLean, M.H. Reilly, M.K. Crawford, E.N. Blanchard, A.Z. Kattamis, S. Wagner. J. Appl. Phys. **102**, *7*, 074512 (2007). https://doi.org/10.1063/1.2786869
[24] H.C.M. Knoops, E. Langereis, M.C.M. van de Sanden, W.M.M. Kessels. J. Electrochem. Soc. **157**, *12*, G241 (2010). https://doi.org/10.1149/1.3491381
[25] J. Lu, J. Aarik, J. Sundqvist, K. Kukli, A. Hårsta, J.-O. Carlsson. J. Cryst. Growth **273**, *3–4*, 510 (2005). https://doi.org/10.1016/j.jcrysgro.2004.09.064
[26] S.M. George, A.W. Ott, J.W. Klaus. J. Phys. Chem. **100**, *31*, 13121 (1996). https://doi.org/10.1021/jp9536763
[27] M. Leskelä, M. Ritala. Thin Solid Films **409**, *1*, 138 (2002). https://doi.org/10.1016/S0040-6090(02)00117-7
[28] R.L. Puurunen. J. Appl. Phys. **97**, *12*, 121301 (2005). https://doi.org/10.1063/1.1940727
[29] V. Miikkulainen, M. Leskelä, M. Ritala, R.L. Puurunen. J. Appl. Phys. **113**, *2*, 21301 (2013). https://doi.org/10.1063/1.4757907
[30] V.A. Gritsenko, T.V. Perevalov, D.R. Islamov. Phys. Rep. **613**, 1 (2016). https://doi.org/10.1016/j.physrep.2015.11.002
[31] T.-C. Tien, L.-C. Lin, L.-S. Lee, C.-J. Hwang, S. Maikap, Y.M. Shulga. J. Mater. Sci.: Mater. Electron. **21**, *5*, 475 (2010). https://doi.org/10.1007/s10854-009-9941-0
[32] K. Yan, W. Yao, Y. Zhao, L. Yang, J. Cao, Y. Zhu. Appl. Surf. Sci. **390**, 260 (2016). https://doi.org/10.1016/j.apsusc.2016.08.051
[33] P. Broqvist, A. Pasquarello. Appl. Phys. Lett. **89**, *26*, 262904 (2006). https://doi.org/10.1063/1.2424441

[34] E.S. Toberer, M. Christensen, B.B. Iversen, G.J. Snyder. Phys. Rev. B **77**, *7*, 075203 (2008). https://doi.org/10.1103/PhysRevB.77.075203
[35] H. Zheng, Z.F. Wang, T. Luo, Q.W. Shi, J. Chen. Phys. Rev. B **75**, *16*, 165414 (2007). https://doi.org/10.1103/PhysRevB.75.165414
[36] J. Robertson. Rep. Progr. Phys. **69**, *2*, 327 (2006). https://doi.org/10.1088/0034-4885/69/2/R02
[37] D. Muñoz Ramo, A.L. Shluger, J.L. Gavartin, G. Bersuker. Phys. Rev. Lett. **99**, *15*, 155504 (2007). https://doi.org/10.1103/PhysRevLett.99.155504
[38] K. Xiong, J. Robertson, M.C. Gibson, S.J. Clark. Appl. Phys. Lett. **87**, *18*, 183505 (2005). https://doi.org/10.1063/1.2119425
[39] D.R. Islamov, V.A. Gritsenko, V.N. Kruchinin, E.V. Ivanova, M.V. Zamoryanskaya, M.S. Lebedev. Phys. Solid State **60**, *10*, 2050 (2018). https://doi.org/10.1134/S1063783418100098
[40] I. Villa, A. Vedda, M. Fasoli, R. Lorenzi, N. Kränzlin, F. Rechberger, G. Ilari, D. Primc, B. Hattendorf, F.J. Heiligtag, M. Niederberger, A. Lauria. Chem. Mater. **28**, *10*, 3245 (2016). https://doi.org/10.1021/acs.chemmater.5b03811
[41] E.V. Ivanova, M.V. Zamoryanskaya, V.A. Pustovarov, V.S. Aliev, V.A. Gritsenko, A.P. Yelisseyev. J. Exp. Theor. Phys. **120**, *4*, 710 (2015). https://doi.org/10.1134/S1063776115020132
[42] Y.M. Strzhemechny, M. Bataiev, S.P. Tumakha, S.H. Goss, C.L. Hinkle, C.C. Fulton, G. Lucovsky, L.J. Brillson. J. Vac. Sci. Technol. B **26**, *1*, 232 (2008). https://doi.org/10.1116/1.2830692
[43] S. Walsh, L. Fang, J.K. Schaeffer, E. Weisbrod, L.J. Brillson. Appl. Phys. Lett. **90**, *5*, 052901 (2007). https://doi.org/10.1063/1.2435585
[44] V.V. Kaichev, E.V. Ivanova, M.V. Zamoryanskaya, T.P. Smirnova, L.V. Yakovkina, V.A. Gritsenko. Eur. Phys. J. Appl. Phys. **64**, *1*, 10302 (2013). https://doi.org/10.1051/epjap/2013130005
[45] A.A. Rastorguev, V.I. Belyi, T.P. Smirnova, L.V. Yakovkina, M.V. Zamoryanskaya, V.A. Gritsenko, H. Wong. Phys. Rev. B **76**, *23*, 235315 (2007). https://doi.org/10.1103/PhysRevB.76.235315
[46] T. Ito, M. Maeda, K. Nakamura, H. Kato, Y. Ohki. J. Appl. Phys. **97**, *5*, 054104 (2005). https://doi.org/10.1063/1.1856220
[47] M. Kong, B. Li, C. Guo, P. Zeng, M. Wei, W. He. Coatings **9**, *5*, 307 (2019). https://doi.org/10.3390/coatings9050307
[48] P. Makuła, M. Pacia, W. Macyk. J. Phys. Chem. Lett. **9**, *23*, 6814 (2018). https://doi.org/10.1021/acs.jpclett.8b02892
[49] S.V. Bulyarski, V.S. Gorelik, G.G. Gusarov, D.A. Koiva, A.V. Lakalin. Optics. Spectroscopy **128**, *5*, 590 (2020). https://doi.org/10.1134/S0030400X20050057

Translated by Ego Translating